



HAL
open science

Aluminum-Based Metal–Organic Frameworks Derived Al₂O₃-Loading Mesoporous Carbon as a Host Matrix for Lithium-Metal Anodes

Shao-Jian Zhang, Jin-Hai You, Jian-De Chen, Yi-Yang Hu, Chuan-Wei Wang, Qian Liu, Yu-Yang Li, Yao Zhou, Jun-Tao Li, Jolanta Światowska, et al.

► **To cite this version:**

Shao-Jian Zhang, Jin-Hai You, Jian-De Chen, Yi-Yang Hu, Chuan-Wei Wang, et al.. Aluminum-Based Metal–Organic Frameworks Derived Al₂O₃-Loading Mesoporous Carbon as a Host Matrix for Lithium-Metal Anodes. ACS Applied Materials & Interfaces, 2019, 11 (51), pp.47939-47947. 10.1021/acsami.9b16363 . hal-03096404

HAL Id: hal-03096404

<https://hal.science/hal-03096404>

Submitted on 4 Jan 2021

HAL is a multi-disciplinary open access archive for the deposit and dissemination of scientific research documents, whether they are published or not. The documents may come from teaching and research institutions in France or abroad, or from public or private research centers.

L'archive ouverte pluridisciplinaire **HAL**, est destinée au dépôt et à la diffusion de documents scientifiques de niveau recherche, publiés ou non, émanant des établissements d'enseignement et de recherche français ou étrangers, des laboratoires publics ou privés.

Aluminum-Based Metal–Organic Frameworks Derived Al₂O₃- Loading Mesoporous Carbon as a Host Matrix for Lithium Metal Anodes

Shao-Jian Zhang,[†] Jin-Hai You,[†] Jian-De Chen,[†] Yi-Yang Hu,[†] Chuan-Wei Wang,[†] Qian Liu,[‡] Yu-Yang Li,[‡] Yao Zhou,^{†,‡} Jun-Tao Li,^{*,†,‡} Jolanta Swiatowska,^{*,§} Ling Huang,[‡] and Shi-Gang Sun^{*,†,‡}

[†] College of Energy and [‡] State Key Lab of Physical Chemistry of Solid Surface, College of Chemistry and Chemical Engineering, Xiamen University, Xiamen 361005, China

[§]PSL Research University, CNRS – Chimie ParisTech, Institut de Recherche de Chimie Paris (IRCP), 11 rue Pierre et Marie Curie, 75005 Paris, France

ABSTRACT: Li-metal anode attracts great focus owing to its ultra-high specific capacity and the lowest redox potential. However, the uncontrolled growth of Li dendrite leads to severe security issues and limited cycle life. Herein, Al₂O₃ loading mesoporous carbon (Al₂O₃@MOF-C) derived from Al-based metal–organic frameworks (Al-MOFs) was investigated as the stable host matrix for Li metal, in which, Al₂O₃ was served as nano seeds for the Li deposition and decrease the Li nucleation overpotential. Except that, the high specific surface area and wide pore distribution can also buffer the volume changes of Li and fasten electron transfer, hence a dendrite-free morphology was observed even after 50 cycles at 2 mA cm⁻². High Li coulombic efficiency of 97.9% after 100 cycles at 1 mA cm⁻², 1 mAh cm⁻², and 97.6% after 50 cycles at 1 mA cm⁻² and 6 mAh cm⁻² were performed by Al₂O₃@MOF-C electrodes. Good performances were also obtained for Li–sulfur and LiFePO₄ batteries. The performances of Al₂O₃@MOF-C@Li were compared with Li foil and Cu@Li in full cell configurations. The electrochemical tests of full cells based on Al₂O₃@MOF-C@Li indicated that this Al-based functional host matrix can enhance the Li-utilization and lead to significant enhancement of the cycling performance of Li anodes.

KEYWORDS: lithium-metal anodes, mesoporous carbon, metal–organic frameworks, Al₂O₃ nano seeds, lithium dendrites

1. INTRODUCTION

Due to the ever-increasing energy consumptions, it is urgent to increase the power and energy density of the lithium-based batteries for further applications. Therefore, rechargeable Li metal batteries (LMBs), like Li–S/Se and Li–air batteries, have attracted extensive attention owing to their ultra-high power density.^{1–6} Li metal has been widely believed as the ideal anode for LMBs because of its ultra-high specific capacity (3860 mAh g⁻¹) and the low redox potential (–3.04 V versus standard hydrogen electrode).⁷ Unfortunately, the Li-metal anodes suffer from an infinite volume changes and thus, an instability of solid electrolyte interface (SEI) layer during the Li plating/stripping process. The volume changes of electrode materials can increase the internal pressure of the cell and cause the modifications at electrode/electrolyte interfaces.⁸ This process is related to the formation of uneven Li electrodeposits called Li dendrites, which can break the solid electrolyte interface (SEI) layer and lead to its reconstitution on the surface of new Li electrodeposits. The Li dendrites not only cause severe loss of active Li leading to a limited cycling lifespan of Li anodes^{9,10} but also might puncture the separator that can result in an internal short circuit of the batteries.¹¹ Therefore, addressing the uneven Li deposition and suppression of the Li dendrite formation are the most crucial issues for the commercialization of the Li-metal anodes.

To overcome these critical issues, many strategies have been adopted to enhance the cycling stability of the Li anodes and decrease the formation of Li dendrites. Electrolyte, containing additives, plays a considerable role in the cycling performances of Li-metal anodes. Surface film-forming additives like LiF,¹² LiPF₆,^{13,13} LiNO₃, and Li₂S_x^{14–17} can induce the formation of desirable SEI layer and stabilize the Li anode. Other functional additives, which contain Cs⁺ and Rb⁺ ions^{18,19} were also investigated to homogenize the Li electrochemical deposition.

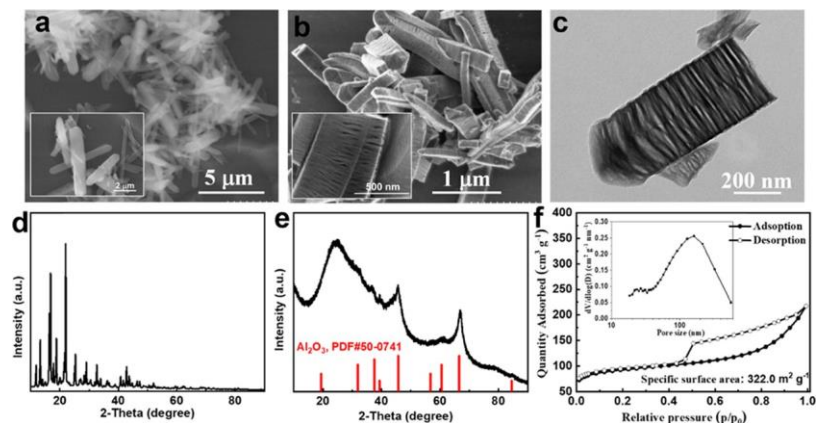


Figure 1. SEM images of the Al-MOF (a) and Al₂O₃@MOF-C (b) and the TEM images of the Al₂O₃@MOF-C (c). XRD patterns of the Al-MOF (d) and Al₂O₃@MOF-C (e) and the N₂ adsorption/desorption isotherms of Al₂O₃@MOF-C (f) and corresponding pore distribution curves (inserted figure in f).

Besides, surface-coating layers, such as phosphate-functionalized reduced graphene oxides,²⁰ lithiophilic-lithiophobic gradient interfacial layer,²¹ LiPON layer,²² agarose film,²³ Li_xSiO_y protective layer,²⁴ and LiF/Li₃N artificial SEI layer²⁵ can serve as the artificial protecting SEI layers to alleviate the formation of the Li dendrites. In addition, the design of threedimensional current collectors, which serves as the hosts of the Li metal arises as another effective strategy in this regard.⁸ On one hand, the use of the host matrices can regulate the local effective current density toward controlling the lithium nuclei size and thus restraining the Li dendrites. On the other hand, the host matrices also can significantly accommodate the huge volume variations during the Li plating/stripping processes. Many three-dimensional hosts for the Li metal have been explored such as Ni@Li₂O Co-axial Nanowire,²⁶ TiC/C core/shell nanowire skeleton,²⁷ AlF₃ frameworks,²⁸ etc. Among them, the carbon-based materials like hollow carbon fibers,²⁹ reduced graphene layers,³⁰ N-doped graphitic carbon foams,³¹ straw-brick-like carbon fiber cloth,³² lithium-graphite hybrid anodes,³³ etc. have been proposed as host matrixes for the Li metal due to their large surface areas and fast electron/Li⁺ transfer. In addition, introducing some lithiophilic sites like MgO,³⁴ CoO,³⁵ ZnO,³⁶ Al₂O₃,³⁴ Ag nanoparticles,³⁷ etc. can significantly decrease the energy barrier of Li nucleation, guide the Li deposition behavior without the formation of dendrites. Towards the pursuit of highly efficient carbon-based host matrix for lithium metal, metal-organic frameworks (MOFs) as a relatively new class of crystalline porous materials with high specific surface area, wide structural diversity, and easy tailorability, have also been widely used as anodes for both lithium- and sodium-ion batteries, ever since the pioneering work by Tarascon et al.³⁸ Afterwards many functional materials derived from the MOFs were prepared to explore their further application in Li-based batteries. Benefitting from large space and integrated carbon matrix, which can buffer the volume variations, the MOFs like NiO,^{39,40} Co₃O₄,⁴¹

Fe₂O₃,⁴² and CuO/Cu₂O⁴³ with yolk shell or hollow structure can be formed by calcination. These MOFs-based materials have been widely investigated for the LIBs.

In this study, Al₂O₃ loading mesoporous carbon (Al₂O₃@MOF-C), which was prepared by pyrolyzing an Al-based metal-organic framework with a chemical formula of Al(OH)(1,4-NDC) 2H₂O (Al-MOFs), was applied as a host matrix for the Li metal. The high specific surface area and wide distribution of the pore size of this material can buffer the volume changes and fasten the electron and ion fluxes. Besides, the Al₂O₃ in the frameworks can serve as nano seeds for the Li nucleation and guide the Li deposition without the dendrites formation. Here, in this work, the coulombic efficiency of Al₂O₃@MOF-C used as a host for Li, was studied by varying the current and capacity. The Li predeposited Al₂O₃@MOF-C (Al₂O₃@MOF-C@Li) was also tested and compared to Li foil and/or Cu@Li with the sulfur/carbon black cathodes or LiFePO₄ cathodes to evaluate the cycling performance in full cells. The morphology and chemical constitution of electrodes were studied by the means of microscopic (scanning electron microscopy (SEM), transmission electron microscopy (TEM)) and spectroscopic techniques (X-ray diffraction (XRD) and Xray photoelectron spectroscopy (XPS)).

2. RESULTS AND DISCUSSION

The SEM images of Al-MOFs (Figure 1a) show a stick-like morphology with a length of about 5–10 μm . The XRD pattern of the Al-MOFs (Figure 1d) confirmed its chemical composition as a pure $\text{Al}(\text{OH})(1,4\text{-NDC})\cdot 2\text{H}_2\text{O}$ material, which is in agreement with the work reported before.⁴⁴ After 6 h of pyrolysis at 900 $^\circ\text{C}$ under the Ar atmosphere, wide stripshaped pores can be observed while its stick-like morphology is well retained (Figure 1b). From the TEM images of $\text{Al}_2\text{O}_3@ \text{MOF-C}$, strip-shaped pores with a length of ~ 130 nm and a width of ~ 10 nm can be clearly observed (Figures 1c and Figure S1a,b). In the XRD pattern, two broad peaks at around 25 and 44 $^\circ$, characteristics of (002) and (101) crystalline planes of graphite are observed (Figure 1e).⁴⁵ Besides, some peaks of the Al_2O_3 phase can be found in the XRD pattern, whose presence can be explained by the formation of Al_2O_3 during the pyrolysis under the atmosphere of Ar flow. The XPS results (Al 2p spectra shown in Figure S2a) also confirm the presence of Al_2O_3 .

Furthermore, the EDS results show that the percentage of Al atoms in $\text{Al}_2\text{O}_3@ \text{MOF-C}$ can be 7.98% (Figure S3), and the

uniform distribution of C, O, and Al elements in the $\text{Al}_2\text{O}_3@ \text{MOF-C}$ also can be well observed from the energy dispersive spectrometer (EDS) mapping (Figure S4). According to the literature reported before, the Al_2O_3 can serve as nano seeds to guide the initial nucleation of Li metal.³⁴ Additionally, the lattice fringes of the graphite can be observed on $\text{Al}_2\text{O}_3@ \text{MOF-C}$ particles (Figure S1c). The Raman spectrum (Figure S2b) of the $\text{Al}_2\text{O}_3@ \text{MOF-C}$ displays two main peaks at around 1350 and 1600 cm^{-1} , which can be separately indexed to the D band and G band of the graphitic. The ratio of the D band and G band is 1.042, demonstrating the high graphitization degree of the $\text{Al}_2\text{O}_3@ \text{MOF-C}$, indicating remarkable electronic conductivity,⁴⁶ which can fasten the electron transfer during the Li plating/stripping process. As depicted in Figure 1f, the $\text{Al}_2\text{O}_3@ \text{MOF-C}$ exhibits a specific surface area of 322.0 $\text{m}^2 \text{g}^{-1}$ and a wide distribution of pore size ranging from 10 to 80

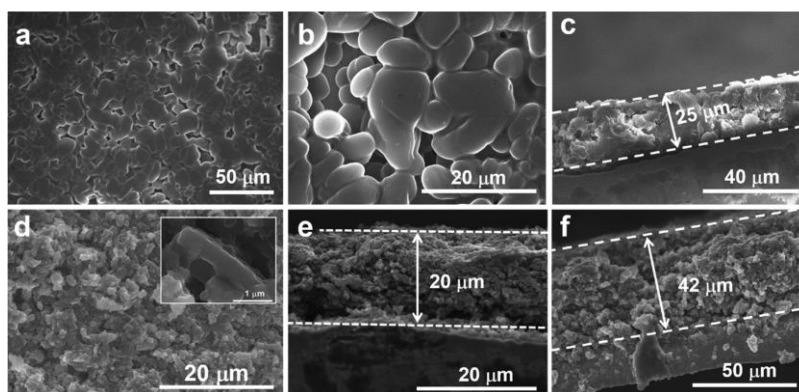


Figure 2. Top-view SEM images of the Cu@Li (a, b), $\text{Al}_2\text{O}_3@ \text{MOF-C}@ \text{Li}$ electrodes (d) and the high-resolution image of $\text{Al}_2\text{O}_3@ \text{MOF-C}@ \text{Li}$ (inserted figure in d). The side-view SEM images of Cu@Li (c), $\text{Al}_2\text{O}_3@ \text{MOF-C}$ (e), and $\text{Al}_2\text{O}_3@ \text{MOF-C}@ \text{Li}$ (f) electrodes after plating 6 mAh cm^{-2} of Li at a current density of 1 mA cm^{-2} .

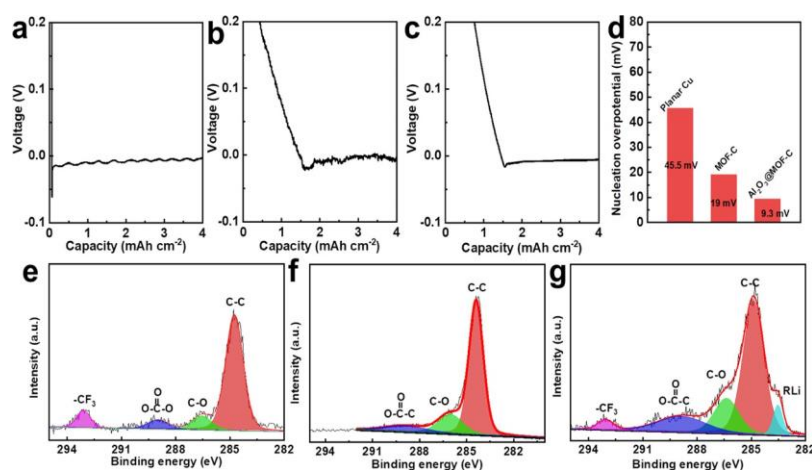


Figure 3. Voltage-capacity curves of the Li deposits on different substrates: (a) planar Cu, (b) MOF-C, and (c) $\text{Al}_2\text{O}_3@ \text{MOF-C}$. Nucleation overpotential on different substrates at 0.2 mA cm^{-2} (d). XPS of C 1s spectra recorded for: (e) the Cu@Li (0.5 mAh cm^{-2}), (f) pristine $\text{Al}_2\text{O}_3@ \text{MOF-C}$, and (g) $\text{Al}_2\text{O}_3@ \text{MOF-C}$ after plating 0.5 mAh cm^{-2} Li.

nm (inserted in Figure 1f). These properties can decrease the local current density and homogenize the formation of the Li nucleus and enable a dendrite-free deposition of the Li metal.

The morphologies of the different substrates (Cu and Al₂O₃@MOF-C substrates) with different amounts of Li plated on them are firstly compared (Figures S5 and S6).

When 0.5 mAh cm⁻² of Li is deposited on the Cu substrate, the Li particles with a diameter of about 2–4 μm can be observed. Further increasing the Li amount on the Cu substrate, the diameter of Li particles grows bigger than before (Figure S5a–c). As for the Al₂O₃@MOF-C substrate, the Li can be well dispersed by the Al₂O₃@MOF-C when the Li amount is 0.5 mAh cm⁻² (Figure S5d). From the higher magnification SEM image, we can see that there are some tiny Li particles deposited on the Al₂O₃@MOF-C particles, indicating that the substrate can enable uniform Li nucleation (Figure S6a). When the Li capacity increases to 6 mAh cm⁻², uniform Li distribution also can be observed (Figure S5e) and the Al₂O₃@MOF-C particles are well covered by the Li metal (Figure S6b). Further elevation of the Li capacity on the Al₂O₃@MOF-C substrate to 8 mAh cm⁻², a Li layer consisted of some Li particles can be formed on the substrate,

meaning the Li capacity is beyond the tolerance of substrate (Figure S5f). The morphologies of 6 mAh cm⁻² of Li deposited on Al₂O₃@MOF-C (Al₂O₃@MOF-C@Li) were investigated and compared to the Li deposited at the same conditions on the planar Cu foil. As observed in Figure 2a,b, the mossy-like Li metal was formed on the Cu foil. This may easily lead to the formation of Li dendrites and excessive formation of the SEI layer after repeated cycles, resulting in poor Li coulombic efficiency and the failure of the cells. The cross-section images of the Cu@Li electrode show that the thickness of the Li layer deposited on the Cu substrate can be about 25 μm (Figure 2c). As we can see from the SEM images of the Al₂O₃@MOF-C electrode, the surface of Al₂O₃@MOF-C is rough and the pore structure of particles are still well maintained (Figure S7). After the deposition of Li, the Li metal can be well dispersed by the Al₂O₃@MOF-C particles and large Li particles cannot be observed (Figure 2d). Furthermore, as one can observe from the cross-section images of the Al₂O₃@MOF-C before and after plating Li metal, the thickness of the host matrix layer increases from 20 to 42 μm, whereas the electrode structure is well maintained (Figure 2e,f). What is more, after stripping the Li as deposited on the Al₂O₃@MOF-C, the host matrixes

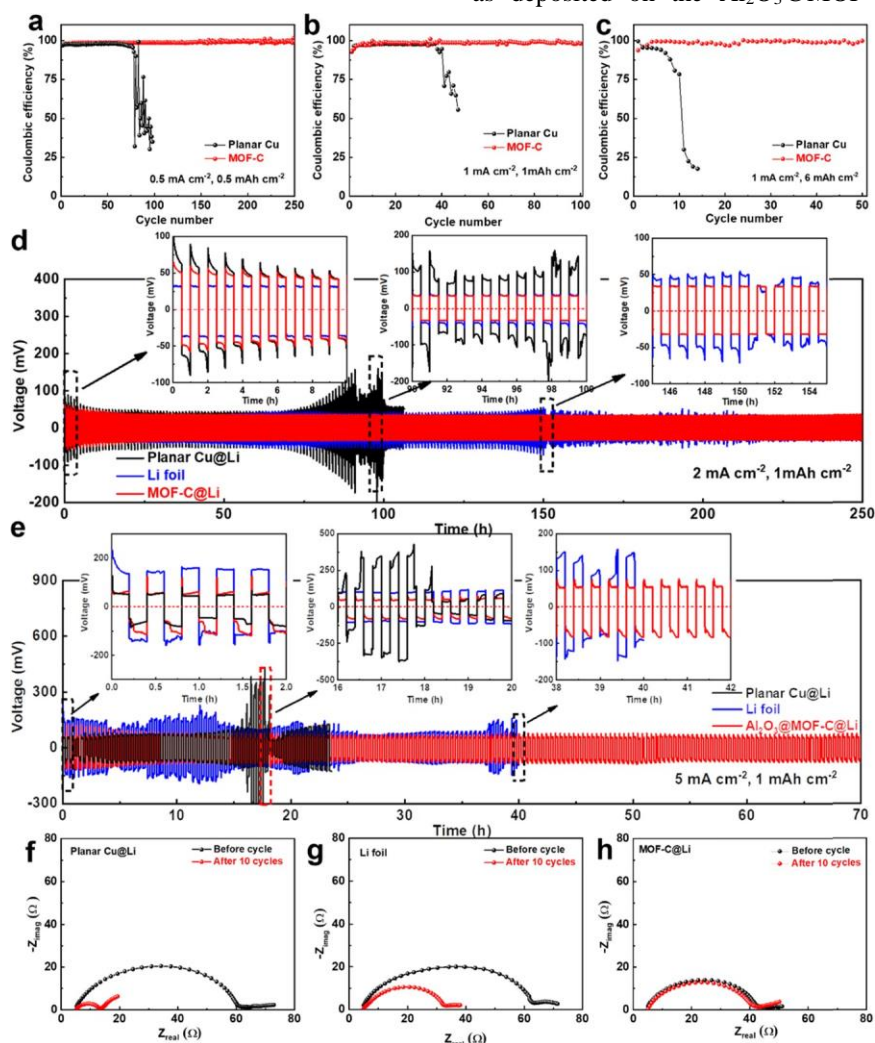


Figure 4. Coulombic efficiency of the cells with planar 6 mAh cm⁻² predeposited Cu and Al₂O₃@MOF-C electrodes: (a) 0.5 mA cm⁻², 0.5 mAh cm⁻², (b) 1 mA cm⁻², 1 mAh cm⁻², and (c) 1 mA cm⁻², 6 mAh cm⁻². The voltage–time profiles of the cells with planar Cu@Li, Li foils, and Al₂O₃@MOF-C@Li electrodes at different current density: (d) 2 mA cm⁻², 1 mAh cm⁻² and (e) 5 mA cm⁻², 1 mAh cm⁻². EIS Nyquist plots performed at OCP before cycling and after 10 cycles: (f) planar Cu@Li, (g) Li foils, and (h) Al₂O₃@MOF-C@Li.

become porous, which may further provide larger space for the following deposition of Li (Figure S8a). And it can be observed from the cross-section of the $\text{Al}_2\text{O}_3@\text{MOF-C}$ host matrixes that the host matrixes still integrated without exfoliation of active particles (Figure S8b). These results indicate that the $\text{Al}_2\text{O}_3@\text{MOF-C}$ host matrixes can well buffer the volume variation during the Li plating/stripping processes, which can guarantee the integrality of the Li anodes.

To explore the effect of the $\text{Al}_2\text{O}_3@\text{MOF-C}$ host matrixes on the initial nucleation stage of Li, the voltage-capacity curves of the Li deposits were used (Figure 3). The Li nucleation overpotential, defined as a gap between the minimum voltage and the voltage of flat plateau, was compared for different substrates. The $\text{Al}_2\text{O}_3@\text{MOF-C}$ exhibits the smallest nucleation overpotential of only 9.3 mV at a current density of 0.5 mA cm^{-2} for the Li plating process (Figure 3c,d). However, the Cu substrate suffers five times higher nucleation overpotential as much as 45.5 mV than that of $\text{Al}_2\text{O}_3@\text{MOF-C}$ (Figure 3a,d). The lowest nucleation potential observed for $\text{Al}_2\text{O}_3@\text{MOF-C}$ can have a significant influence on homogenous initial nucleation of Li (Figure 3c,d). To investigate the function of Al_2O_3 in the host matrix, we removed the Al_2O_3 in $\text{Al}_2\text{O}_3@\text{MOF-C}$ by treatment of 2 M HCl solution to generate an Al_2O_3 -free host matrix (MOF-C). After etching, the XRD pattern of the MOF-C only shows two broad peaks for graphite (Figure S9a). Besides, from the XPS survey spectra, the lower intensity of Al 2p can be observed for MOF-C than that for $\text{Al}_2\text{O}_3@\text{MOF-C}$, which also demonstrates that the Al_2O_3 can be removed by HCl solution (Figure S9b). SEM presented in Figure S10 shows that the stick-like particles with wide strip-shaped pores morphology of MOF-C is not modified by the HCl etching and its specific surface area is increased to $335.4 \text{ m}^2 \text{ g}^{-1}$ (Figure S11). From the deposition curve of Li on MOF-C substrate, we can see that the overpotential is 19 mV, which is higher than $\text{Al}_2\text{O}_3@\text{MOFC}$ (Figure 3c,d). Summarizing, the lower nucleation overpotential observed for $\text{Al}_2\text{O}_3@\text{MOF-C}$ than that for MOF-C can be related to high quantity of Al_2O_3 phase in the matrixes enables easier and more efficient Li nucleation, indicating that the Al_2O_3 plays a crucial role in the Li metal growth.

Except that, we also performed the XPS to analyze the interaction between $\text{Al}_2\text{O}_3@\text{MOF-C}$ and Li metal. Before the XPS characterization, 0.5 mAh cm^{-2} Li metal was plated on the planar Cu and $\text{Al}_2\text{O}_3@\text{MOF-C}$ substrates. As illustrated in Figure 3e, the following C-like species C-C/C-H (284.5 eV), C-O (286.5 eV), $-\text{CO}_3$ (289.0 eV), and $-\text{CF}_3$ (293 eV) can be found on the Cu@Li (0.5 mAh cm^{-2}) surface. The lower binding energy peaks (at 284.5 eV and at 286.5 eV) can be typical C-like surface contaminants, and the higher binding energy peaks attributed to $-\text{CO}_3$ and to $-\text{CF}_3$ ⁴⁶⁻⁴⁸ can be the components of the SEI layer in agreement with the literature.^{49,50} It cannot be completely ruled out that a particularly broad peak at 289.0 eV

corresponding to $-\text{CO}_3$ (observed for $\text{Al}_2\text{O}_3@\text{MOF-C}$ after plating in Figure 3g) could be decomposed to two peaks assigned to organic lithium alkyl carbonates (ROCO_2Li) and lithium carbonates (Li_2CO_3).⁵¹ Compared with the pristine $\text{Al}_2\text{O}_3@\text{MOF-C}$ (Figure 3f), the $\text{Al}_2\text{O}_3@\text{MOF-C@Li}$ (0.5 mAh cm^{-2}) (Figure 3g) exhibits the presence of $-\text{CF}_3$ group, which originates from the electrolyte decomposition, particularly the LiTFSI salt.^{51,52} A new component at a low binding energy of around 283.2 eV attributed to lithium carbide species (R-Li)^{53,54} can be detected on $\text{Al}_2\text{O}_3@\text{MOF-C@Li}$ (0.5 mAh cm^{-2}) and not on Cu@Li (0.5 mAh cm^{-2}), indicating the strong interaction between the carbon matrix and Li metal. This interaction might influence a homogenous growth of the Li nuclei.

The Li coulombic efficiency of the $\text{Al}_2\text{O}_3@\text{MOF-C}$ electrode was evaluated by means of galvanostatic discharge/charge profiles, and it was compared against that of the planar Cu electrode (Figure 4). A constant capacity of 1 mAh cm^{-2} was applied for the Li plating process while 0.5 V was employed as the upper cut-off voltage for the Li stripping, and the Li coulombic efficiency was calculated from the lithium ratio between the Li plating and stripping process. The $\text{Al}_2\text{O}_3@\text{MOF-C}$ electrode can deliver a coulombic efficiency as high as 99.3% at 0.5 mA cm^{-2} and 0.5 mAh cm^{-2} after 250 cycles (Figure 4a). When the current density and Li capacity were elevated to 1 mA cm^{-2} and 1 mAh cm^{-2} for the Li plating process, the coulombic efficiency reached 97.9% after 100 cycles, which is obviously superior to the Cu-based anode suffering from a sudden decrease after 40 cycles under the same conditions (Figure 4b). Moreover, when the capacity of Li metal for the Li plating process was fixed at 6 mAh cm^{-2} , a high coulombic efficiency was obtained for 50 cycles by using $\text{Al}_2\text{O}_3@\text{MOF-C}$ substrate (Figure 4c). The high coulombic efficiency demonstrates that the $\text{Al}_2\text{O}_3@\text{MOF-C}$ can significantly obstruct the formation of the dead Li, which is beneficial to access an extended cycling life of the Li-metal anodes. Moreover, the cycling performances of the planar Cu@Li and $\text{Al}_2\text{O}_3@\text{MOF-C@Li}$ electrodes were compared in cells with the commercial Li foil as the counter electrode. Both planar Cu and $\text{Al}_2\text{O}_3@\text{MOF-C}$ electrodes were predeposited with 6 mAh cm^{-2} of Li at a current density of 0.5 mA cm^{-2} . The voltage-time profiles, which record the variation of voltage of the Li plating/stripping processes under fixed current density and Li capacity, were applied to monitor any instability in the cells. The voltage-time profiles of the cells at current densities of 1, 2, and 5 mA cm^{-2} are shown in Figures S12 and 4d,e. The planar Cu@Li electrode suffered from a sudden increase in the hysteresis at about 80 h (40 cycles) at 1 mA cm^{-2} , resulted from an impedance rise during the plating/stripping process, and then the voltage dropped sharply at 110 h (55 cycles). Such a huge potential drop indicates the short circuit of the cells caused by the ever-growth of Li dendrites punctures the separator.⁵¹ In addition, the planar Cu@Li electrodes delivered only a

limited lifespan of 70 h (70 cycles) at 2 mA cm^{-2} and 1 mAh cm^{-2} and only 15 h (~ 38 cycles) at 5 mA cm^{-2} and 1 mAh cm^{-2} . In comparison, the $\text{Al}_2\text{O}_3@ \text{MOF-C@Li}$ electrodes delivered a much more stable cycling performance. At 1 mA cm^{-2} , 1 mAh cm^{-2} , in the first cycle, a lower hysteresis of $\sim 30 \text{ mV}$ for $\text{Al}_2\text{O}_3@ \text{MOF-C@Li}$ electrodes was observed and the hysteresis only increased slightly after 500 h (250 cycles). Similarly, the $\text{Al}_2\text{O}_3@ \text{MOF-C@Li}$ electrodes showed a hysteresis of $\sim 50 \text{ mV}$ at 2 mA cm^{-2} and 1 mAh cm^{-2} for 250 h (250 cycles). Except that, even at 5 mA cm^{-2} , the $\text{Al}_2\text{O}_3@ \text{MOF-C@Li}$ electrode also showed a stable cycling performance for 175 cycles (70 h). For the sake of comparison, we also performed the Li symmetric cells, by using two Li foils as the electrodes. However, the hysteresis of the Li symmetric cell at 1 mA cm^{-2} , 1 mAh cm^{-2} is obviously increased at $\sim 270 \text{ h}$ (135 cycles), and becomes fluctuant after 150 h (150 cycles) when the current density increases to 2 mA cm^{-2} and 1 mAh cm^{-2} . To further investigate the function of Al_2O_3 in the host matrix, the cycling performance of MOF-C@Li also be carried out. After removing Al_2O_3 from the host matrix, the MOF-C@Li exhibits a shorter lifespan of about 170 h (170 cycles), which is less than that of $\text{Al}_2\text{O}_3@ \text{MOF-C@Li}$ (over 250 cycles) at 2 mA cm^{-2} and 1 mAh cm^{-2} (Figure S13). To illustrate this result, nano Al_2O_3 was coated on the Cu collectors ($\text{Al}_2\text{O}_3@ \text{Cu}$) to investigate the function of Al_2O_3 to assist better cycling performance. As shown in Figure S14, the $\text{Al}_2\text{O}_3@ \text{Cu@Li}$ can maintain stable Li plating/stripping processes for over 160 cycles at 2 mA cm^{-2} and 1 mAh cm^{-2} , which is much better than that of planar Cu@Li (70 cycles), indicating that the Al_2O_3 in the host matrix may contribute to better cycling stability.

Except that, the performances of different Li anodes also are estimated in the carbonate-based electrolyte (1 M LiPF_6 in ethylene carbonate/dimethyl carbonate (EC/DMC) (1/1 v/v) with 5% FEC). As we can see from Figure S15, the $\text{Al}_2\text{O}_3@ \text{MOF-C@Li}$ can deliver a voltage hysteresis of about 70 mV and stable performance can be maintained for over 200 h (125 cycles) at 1 mA cm^{-2} , 1 mAh cm^{-2} . On the contrary, the Cu@Li and Li foil exhibit higher hysteresis of 70 and 90 mV, respectively. And only after 35 cycles, a significant drop in voltage occurs in the cell with Cu@Li , indicating the internal short circuit of the cell. Similarly, the Li foil also has a limited lifespan of only 90 cycles. These results indicate that a longer lifespan and a stable cycling performance of Li-metal anode can be achieved by using $\text{Al}_2\text{O}_3@ \text{MOF-C}$ as the host matrix.

Electrochemical impedance was also carried out to investigate the interfacial stability of cells with different electrodes. As one can observe from Figure 4f, the total impedance is about 60Ω and drops to 15Ω after 10 cycles. This could be related to the gradual increase of the specific surface area due to the growth of Li dendrites.⁵⁵ For the Li foils (Figure 4g), a similar impedance as observed for the planar Cu@Li electrode can be observed before cycling.

After 10 cycles, the drop of the impedance also indicates the formation of Li dendrites (Figure 4g). However, the $\text{Al}_2\text{O}_3@ \text{MOF-C}$ (Figure 4h) reveals a smaller impedance of only 43Ω before cycling, due to the large specific surface area and fast electron and ion transfer. Only a slight impedance increase can be observed after 10 cycles (Figure 4h). These results demonstrate that the $\text{Al}_2\text{O}_3@ \text{MOF-C}$ can decrease the electrolyte decomposition and enhance interfacial stability.

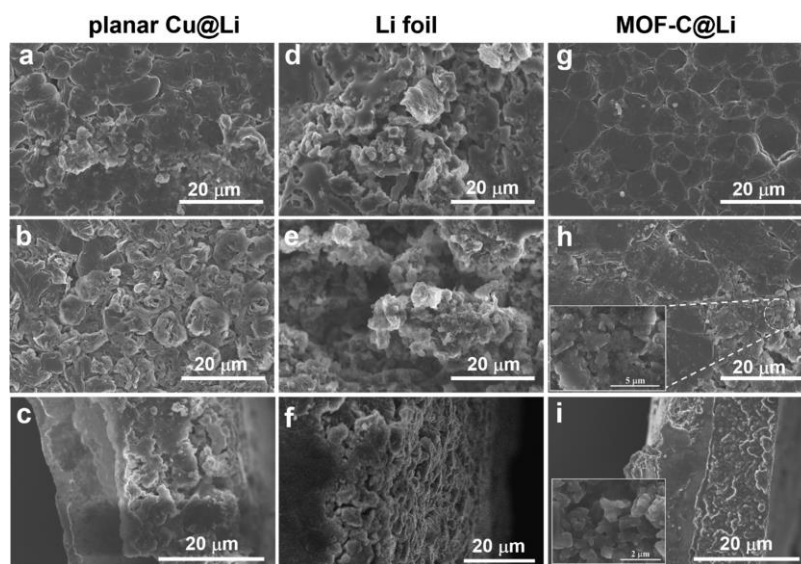


Figure 5. Top-view SEM images of the planar Cu@Li (a, b), Li foils (d, e), Al₂O₃@MOF-C@Li (g, h), and the high-resolution image of Al₂O₃@MOF-C@Li (inserted figure in h) at a current density of 2 mA cm⁻²: (a, d, g) 20 cycles and (b, e, h) 50 cycles. And the side-view SEM images of planar Cu@Li (c), Li foils (f), Al₂O₃@MOF-C@Li (i) and the high-resolution image of Al₂O₃@MOF-C@Li (inserted figure in i) at current density of 2 mA cm⁻² for 50 cycles.

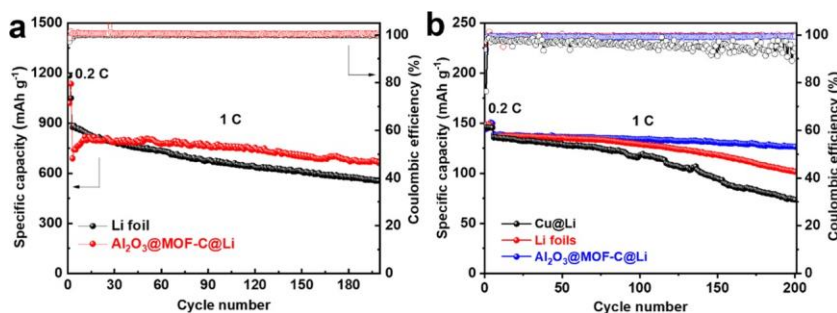


Figure 6. Cycling performances of the (a) Li-S and (b) Li/LiFePO₄ cells using different Li-metal anodes.

The morphology of the planar Cu@Li, Li foils, and Al₂O₃@MOF-C@Li cycled at 2 mA cm⁻² was characterized by SEM. The planar Cu@Li shows a rough surface with some Li metal detachment after 20 cycles (Figure 5a), however, after 50 cycles (Figure 5d), more significant modifications and dendrite-like Li metal can be clearly observed. Similar morphology of Li anode with uneven growth of mossy lithium can be observed after 20 cycles (Figure 5b) and the severe growth of Li dendrites after 50 cycles (Figure 5e). However, the Al₂O₃@MOF-C@Li electrodes exhibit a smooth and flat morphology after 20 cycles (Figure 5c) and after 50 cycles (Figure 5f), dendritic Li still cannot be observed. The sideview SEM images of planar Cu@Li, Li foils, and Al₂O₃@MOF-C@Li electrodes after 50 cycles (Figure 5g-i) also demonstrate the even and dendrite-free morphology on the Al₂O₃@MOF-C@Li electrode. The smoother Li surface on the Al₂O₃@MOF-C substrates after cycles can be attributed to the multifunctional effects of the Al₂O₃@MOF-C substrates. In which, Al₂O₃ nano seeds help homogenize the initial Li nucleation, and porous structure with high surface area and

wide pore distribution provides enough space and decrease the efficient current density for Li deposition.

To evaluate the further application of these Li anodes in Li-S and Li-ion batteries, the additional tests were performed in full cell configurations (Figure 6). To do so, the Al₂O₃@MOF-C@Li anodes were used and compared with Li foils and additionally for Li-ion full cell the comparison was also done with Li deposited on the planar Cu substrate. For the cathode material of the lithium-sulfur batteries, the acetylene black was used as the sulfur host matrix. The sulfur loading rate was 70% and 1675 mA g⁻¹ was defined as 1C. As shown in Figure 6a, the cell with Li foil can deliver an initial capacity of 875.6 mAh g⁻¹ at 1C and suffers a severe capacity loss after cycles with a specific capacity of only 556.4 mAh g⁻¹ after 200 cycles. The cell with Al₂O₃@MOF-C@Li shows a gradual increase in the inceptive cycles and reaches the highest capacity (820.2 mAh g⁻¹) at 20th cycle. After 200 cycles at 1C, the cell with Al₂O₃@MOF-C@Li anode can still perform a capacity as high as 665.6 mAh g⁻¹, associated to a capacity retention of 81.1%, which is notably higher than that with Li foil (63.5%).

For the cathode material in Li-ion full cell, the commercial LiFePO₄ cathode was employed to evaluate the contribution of the Al₂O₃@MOF-C host matrix in elevating the performance of Li anodes (Figure 6b). A similar specific capacity of approximately 145 mAh g⁻¹ at 0.2C (1C = 170 mAh g⁻¹) was observed when using different Li anodes, and decrease to about 138 mAh g⁻¹ when charging/discharging rate increased to 1C. Nevertheless, the LiFePO₄ full cells with Cu@Li and Li foils suffer a serious decay after following cycles with capacity retention of 74.8 and 54.2% after 200 cycles at 1C, respectively. On the contrary, the LiFePO₄ full cell with Al₂O₃@MOF-C@Li delivers an initial capacity of 138.8 mAh g⁻¹ and only slightly fades to 126.5 mAh g⁻¹ after 200 cycles, corresponding to capacity retention as high as 91.1%. Thus, it can be concluded that the Al₂O₃@MOF-C@Li anodes can be considered as promising anodes for the Li-metal batteries with a prolonged cycling lifespan.

3. CONCLUSIONS

The Al₂O₃@MOF-C with a high surface area and wide pore distribution was investigated as the stable host for Li-metal anode in this study. The Al₂O₃ nano seeds and wellconductivity carbon frameworks can guide the Li deposition and decrease the local current density of Li deposition and dissolution, hence a dendrite-free surface can be observed even after 50 Li plating/stripping cycles. Besides, the Al₂O₃@MOFC electrodes can deliver a high Li coulombic efficiency of 97.9% after 100 cycles at a current density of 1 mA cm⁻² and a fixed Li capacity of 1 mAh cm⁻². A high Li coulombic efficiency of 97.6% still can be achieved after 50 cycles even at increased Li capacity to 6 mAh cm⁻², indicating a significant suppression of the dead Li. Except that, the excellent cycling life of Al₂O₃@MOF-C@Li electrodes (250 cycles at 2 mA cm⁻², 175 cycles at 5 mA cm⁻²) confirms high Li utilization during cycling. Furthermore, the enhanced electrochemical performance of the Li-S and Li/LiFePO₄ batteries also demonstrate a potential interesting application of the Al₂O₃@MOF-C@Li anodes. It can be concluded that the Al₂O₃@MOF-C@Li can greatly enhance the cycling performance of Li-metal anodes and promote the development of nextgeneration rechargeable Li-metal batteries.

* Supporting Information

The Supporting Information is available free of charge at <https://pubs.acs.org/doi/10.1021/acsami.9b16363>.

Details for the material preparation, characterization and electrochemical tests; the TEM images of the Al₂O₃@MOF-C powder; Al 2p XPS spectrum and Raman spectrum of the Al₂O₃@MOF-C; EDS spectra and mapping results of the Al₂O₃@MOF-C; the SEM images of Li morphology on different substrates with increasing

Li amount; the SEM images of Al₂O₃@MOF-C electrode; the SEM images of Al₂O₃@MOF-C after first Li plating/stripping cycle; XRD pattern of the MOF-C and XPS survey spectrum of the pristine Al₂O₃@MOF-C and MOF-C; the SEM images of the MOF-C; the N₂ adsorption/desorption isotherms and corresponding pore distribution curves of MOF-C; the voltage-time profiles of cells with different Li anodes at 1 mA cm⁻², 1 mAh cm⁻²; the voltage-time profile of MOF-C@Li at 2 mA cm⁻², 1 mAh cm⁻²; the voltage-time profile of Al₂O₃@Cu@Li at 2 mA cm⁻², 1 mAh cm⁻²; and the voltage-time profiles of the cells with different Li anodes in carbonate-based electrolyte (1 M LiPF₆ in EC/DMC (1/1 v/v) with 5% FEC) at 1 mA cm⁻², 1 mAh cm⁻² (PDF)

AUTHOR INFORMATION

Corresponding Authors

*E-mail: jtli@xmu.edu.cn (J.-T.L.).

*E-mail: jolanta.swiatowska@chimie-paristech.fr (J.S.).

*E-mail: sgsun@xmu.edu.cn (S.-G.S.).

ACKNOWLEDGMENTS

This work was supported by the National Natural Science Foundation of China (21875197, 21621091) and the National Key Research and Development of China (2016YFB0100202).

REFERENCES

- (1) Bruce, P. G.; Freunberger, S. A.; Hardwick, L. J.; Tarascon, J. M. Li-O₂ and Li-S Batteries with High Energy Storage. *Nat. Mater.* 2011, 11, 19–29.
- (2) Song, M. K.; Cairns, E. J.; Zhang, Y. Lithium/Sulfur Batteries with High Specific Energy: Old Challenges and New Opportunities. *Nanoscale* 2013, 5, 2186–2204.
- (3) Ji, X.; Nazar, L. F. Advances in Li-S Batteries. *J. Mater. Chem.* 2010, 20, 9821.
- (4) Abouimrane, A.; Dambournet, D.; Chapman, K. W.; Chupas, P. J.; Weng, W.; Amine, K. A New Class of Lithium and Sodium Rechargeable Batteries Based on Selenium and Selenium-Sulfur as a Positive Electrode. *J. Am. Chem. Soc.* 2012, 134, 4505–4508.
- (5) Yin, Y. X.; Xin, S.; Guo, Y. G.; Wan, L. J. Lithium-Sulfur Batteries: Electrochemistry, Materials, and Prospects. *Angew. Chem., Int. Ed.* 2013, 52, 13186–13200.
- (6) Liu, B.; Fang, R. Y.; Xie, D.; Zhang, W. K.; Huang, H.; Xia, Y.; Wang, X. L.; Xia, X. H.; Tu, J. P. Revisiting Scientific Issues for Industrial Applications of Lithium-Sulfur Batteries. *Energy Environ. Mater.* 2018, 1, 196–208.
- (7) Tarascon, J. M.; Armand, M. Issues and Challenges Facing Rechargeable Lithium Batteries. *Nature* 2001, 414, 359–367.
- (8) Lin, D.; Liu, Y.; Liang, Z.; Lee, H. W.; Sun, J.; Wang, H.; Yan, K.; Xie, J.; Cui, Y. Layered Reduced Graphene Oxide with

Nanoscale Interlayer Gaps as a Stable Host for Lithium Metal Anodes. *Nat. Nanotechnol.* 2016, 11, 626–632.

(9) Lu, D.; Shao, Y.; Lozano, T.; Bennett, W. D.; Graff, G. L.; Polzin,

B.; Zhang, J.; Engelhard, M. H.; Saenz, N. T.; Henderson, W. A.; Bhattacharya, P.; Liu, J.; Xiao, J. Failure Mechanism for Fast-Charged Lithium Metal Batteries with Liquid Electrolytes. *Adv. Energy Mater.* 2015, 5, No. 1400993.

(10) Harry, K. J.; Hallinan, D. T.; Parkinson, D. Y.; MacDowell, A. A.; Balsara, N. P. Detection of Subsurface Structures Underneath Dendrites Formed on Cycled Lithium Metal Electrodes. *Nat. Mater.* 2014, 13, 69–73.

(11) Kim, H.; Jeong, G.; Kim, Y. U.; Kim, J. H.; Park, C. M.; Sohn, H. J. Metallic Anodes for Next Generation Secondary Batteries. *Chem. Soc. Rev.* 2013, 42, 9011–9034.

(12) Lu, Y.; Tu, Z.; Archer, L. A. Stable Lithium Electrodeposition in Liquid and Nanoporous Solid Electrolytes. *Nat. Mater.* 2014, 13, 961–969.

(13) Zheng, J.; Engelhard, M. H.; Mei, D.; Jiao, S.; Polzin, B. J.; Zhang, J. G.; Xu, W. Electrolyte Additive Enabled Fast Charging and Stable Cycling Lithium Metal Batteries. *Nat. Energy* 2017, 2, No. 17012.

(14) Li, W.; Yao, H.; Yan, K.; Zheng, G.; Liang, Z.; Chiang, Y. M.; Cui, Y. The Synergetic Effect of Lithium Polysulfide and Lithium Nitrate to Prevent Lithium Dendrite Growth. *Nat. Commun.* 2015, 6, No. 7436.

(15) Xiong, S.; Xie, K.; Diao, Y.; Hong, X. Characterization of the Solid Electrolyte Interphase on Lithium Anode for Preventing the Shuttle Mechanism in Lithium–Sulfur Batteries. *J. Am. Chem. Soc.* 2014, 246, 840–845.

(16) Cheng, X. B.; Yan, C.; Chen, X.; Guan, C.; Huang, J. Q.; Peng, H. J.; Zhang, R.; Yang, S. T.; Zhang, Q. Implantable Solid Electrolyte Interphase in Lithium–Metal Batteries. *Chem* 2017, 2, 258–270.

(17) Cheng, X. B.; Yan, C.; Peng, H. J.; Huang, J. Q.; Yang, S. T.; Zhang, Q. Sulfurized Solid Electrolyte Interphases with a Rapid Li^+ Diffusion on Dendrite-Free Li Metal Anodes. *Energy Storage Mater.* 2018, 10, 199–205.

(18) Ding, F.; Xu, W.; Graff, G. L.; Zhang, J.; Sushko, M. L.; Chen, X.; Shao, Y.; Engelhard, M. H.; Nie, Z.; Xiao, J.; Liu, X.; Sushko, P. V.; Liu, J.; Zhang, J. G. Dendrite-Free Lithium Deposition via Self-Healing Electrostatic Shield Mechanism. *J. Am. Chem. Soc.* 2013, 135, 4450–4456.

(19) Zhang, Y.; Qian, J.; Xu, W.; Russell, S. M.; Chen, X.; Nasybulin, E.; Bhattacharya, P.; Engelhard, M. H.; Mei, D.; Cao, R.; Ding, F.; Cresce, A. V.; Xu, K.; Zhang, J. G. Dendrite-Free Lithium Deposition with Self-Aligned Nanorod Structure. *Nano Lett.* 2014, 14, 6889–6896.

(20) Kim, M. S.; Ryu, J. H.; Deepika; Lim, Y. R.; Nah, I. W.; Lee, K. R.; Archer, L. A.; Cho, W. I. Langmuir–Blodgett Artificial Solid Electrolyte Interphases for Practical Lithium Metal Batteries. *Nat. Energy* 2018, 3, 889–898.

(21) Zhang, H.; Liao, X.; Guan, Y.; Xiang, Y.; Li, M.; Zhang, W.; Zhu, X.; Ming, H.; Lu, L.; Qiu, J.; Huang, Y.; Cao, G.; Yang, Y.; Mai, L.; Zhao, Y.; Zhang, H. Lithiophilic–Lithiophobic Gradient Interfacial Layer for a Highly Stable Lithium Metal Anode. *Nat. Commun.* 2018, 9, No. 3729.

(22) Wang, W.; Yue, X.; Meng, J.; Wang, J.; Wang, X.; Chen, H.; Shi, D.; Fu, J.; Zhou, Y.; Chen, J.; Fu, Z. Lithium Phosphorus Oxynitride as an Efficient Protective Layer on Lithium Metal Anodes for Advanced Lithium–Sulfur Batteries. *Energy Storage Mater.* 2019, 18, 414–422.

(23) Zhang, S. J.; Gao, Z. G.; Wang, W. W.; Lu, Y. Q.; Deng, Y. P.; You, J. H.; Li, J. T.; Zhou, Y.; Huang, L.; Zhou, X. D.; Sun, S. G. A Natural Biopolymer Film as a Robust Protective Layer to Effectively Stabilize Lithium–Metal Anodes. *Small* 2018, 14, No. e1801054.

(24) Liu, F.; Xiao, Q.; Wu, H. B.; Shen, L.; Xu, D.; Cai, M.; Lu, Y. Fabrication of Hybrid Silicate Coatings by a Simple Vapor Deposition Method for Lithium Metal Anodes. *Adv. Energy Mater.* 2018, 8, No. 1701744.

(25) Liu, S. F.; Xia, X. H.; Deng, S. J.; Xie, D.; Yao, Z. J.; Zhang, L. Y.; Zhang, S. Z.; Wang, Z. L.; Tu, J. P. In Situ Solid Electrolyte Interphase from Spray Quenching on Molten Li: A New Way to Construct High-Performance Lithium–Metal Anodes. *Adv. Mater.* 2018, 31, No. 1806470.

(26) Zou, P.; Chiang, S. W.; Li, J.; Wang, Y.; Wang, X.; Wu, D.; Nairan, A.; Kang, F.; Yang, C. Ni@Li₂O Co-axial Nanowire Based Reticular Anode: Tuning Electric Field Distribution for Homogeneous Lithium Deposition. *Energy Storage Mater.* 2019, 18, 155–164. (27) Liu, S.; Xia, X.; Zhong, Y.; Deng, S.; Yao, Z.; Zhang, L.; Cheng, X. B.; Wang, X.; Zhang, Q.; Tu, J. 3D TiC/C Core/Shell Nanowire Skeleton for Dendrite-Free and Long-Life Lithium Metal Anode. *Adv. Energy Mater.* 2017, 8, No. 1702322.

(28) Wang, H.; Lin, D. C.; Liu, Y. Y.; Li, Y. Z.; Cui, Y. Ultrahigh-Current Density Anodes with Interconnected Li Metal Reservoir Through Overlithiation of Mesoporous AlF₃ Framework. *Sci. Adv.* 2017, 3, No. e1701301.

(29) Liu, L.; Yin, Y. X.; Li, J. Y.; Li, N. W.; Zeng, X. X.; Ye, H.; Guo, Y. G.; Wan, L. J. Free-Standing Hollow Carbon Fibers as High-Capacity Containers for Stable Lithium Metal Anodes. *Joule* 2017, 1, 563–575.

(30) Wang, A.; Tang, S.; Kong, D.; Liu, S.; Chiou, K.; Zhi, L.; Huang, J.; Xia, Y. Y.; Luo, J. Bending-Tolerant Anodes for Lithium Metal Batteries. *Adv. Mater.* 2018, 30, No. 1703891.

(31) Liu, L.; Yin, Y. X.; Li, J. Y.; Wang, S. H.; Guo, Y. G.; Wan, L. J. Uniform Lithium Nucleation/Growth Induced by Lightweight Nitrogen-Doped Graphitic Carbon Foams for High-Performance Lithium Metal Anodes. *Adv. Mater.* 2018, 30, No. 1706216.

(32) Liu, S. F.; Xia, X. H.; Yao, Z. J.; Wu, J. B.; Zhang, L. Y.; Deng, S. J.; Zhou, C. G.; Shen, S. H.; Wang, X. L.; Tu, J. P. Straw-Brick-Like Carbon Fiber Cloth/Lithium Composite Electrode as an Advanced Lithium Metal Anode. *Small Methods* 2018, 2, No. 1800035.

(33) Liu, S. F.; Xia, X. H.; Deng, S. J.; Zhang, L. Y.; Li, Y. Q.; Wu, J. B.; Wang, X. L.; Tu, J. P. Large-Scale Synthesis of High-Quality Lithium–Graphite Hybrid Anodes for Mass-Controllable and Cycling-Stable Lithium Metal Batteries. *Energy Storage Mater.* 2018, 15, 31–36.

(34) Jin, C.; Sheng, O.; Lu, Y.; Luo, J.; Yuan, H.; Zhang, W.; Huang, H.; Gan, Y.; Xia, Y.; Liang, C.; Zhang, J.; Tao, X. Metal Oxide Nanoparticles Induced Step-Edge Nucleation of Stable Li Metal Anode Working under an Ultrahigh Current Density of 15 mA cm⁻². *Nano Energy* 2018, 45, 203–209.

(35) Yue, X. Y.; Wang, W. W.; Wang, Q. C.; Meng, J. K.; Zhang, Z. Q.; Wu, X. J.; Yang, X. Q.; Zhou, Y. N. CoO Nanofiber Decorated Nickel Foams as Lithium Dendrite Suppressing Host Skeletons for High Energy Lithium Metal Batteries. *Energy Storage Mater.* 2018, 14, 335–344.

(36) Wang, L.; Zhu, X.; Guan, Y.; Zhang, J.; Ai, F.; Zhang, W.; Xiang, Y.; Vijayan, S.; Li, G.; Huang, Y.; Cao, G.; Yang, Y.; Zhang, H. ZnO/Carbon Framework Derived from Metal–Organic

- Frameworks as a Stable Host for Lithium Metal Anodes. *Energy Storage Mater.* 2018, 11, 191–196.
- (37) Yang, C.; Yao, Y.; He, S.; Xie, H.; Hitz, E.; Hu, L. Ultrafine Silver Nanoparticles for Seeded Lithium Deposition Toward Stable Lithium Metal Anode. *Adv. Mater.* 2017, 29, No. 1702714.
- (38) Ferey, G.; Millange, F.; Morcrette, M.; Serre, C.; Doublet, M. L.; Greneche, J. M.; Tarascon, J. M. Mixed-Valence Li/Fe-Based Metal-Organic Frameworks with Both Reversible Redox and Sorption Properties. *Angew. Chem., Int Ed.* 2007, 46, 3259–3263.
- (39) Liu, L.; Guo, H.; Liu, J.; Qian, F.; Zhang, C.; Li, T.; Chen, W.; Yang, X.; Guo, Y. Self-Assembled Hierarchical Yolk-Shell Structured NiO@C from Metal-Organic Frameworks with Outstanding Performance for Lithium Storage. *Chem. Commun.* 2014, 50, 9485–9488.
- (40) Zou, F.; Chen, Y. M.; Liu, K.; Yu, Z.; Liang, W.; Bhaway, S. M.; Gao, M.; Zhu, Y. Metal Organic Frameworks Derived Hierarchical Hollow NiO/Ni/Graphene Composites for Lithium and Sodium Storage. *ACS Nano* 2016, 10, 377–386.
- (41) Li, C.; Chen, T.; Xu, W.; Lou, X.; Pan, L.; Chen, Q.; Hu, B. Mesoporous Nanostructured Co₃O₄ Derived from MOF Template: a High-Performance Anode Material for Lithium-Ion Batteries. *J. Mater. Chem. A* 2015, 3, 5585–5591.
- (42) Zhang, L.; Wu, H. B.; Lou, X. W. Iron-Oxide-Based Advanced Anode Materials for Lithium-Ion Batteries. *Adv. Energy Mater.* 2014, 4, No. 1300958.
- (43) Zhang, X.; Qin, W.; Li, D.; Yan, D.; Hu, B.; Sun, Z.; Pan, L. Metal-Organic Framework Derived Porous CuO/Cu₂O Composite Hollow Octahedrons as High Performance Anode Materials for Sodium Ion Batteries. *Chem. Commun.* 2015, 51, 16413–16416.
- (44) Comotti, A.; Bracco, S.; Sozzani, P.; Horike, S.; Matsuda, R.; Chen, J. X.; Takata, M.; Kubota, Y.; Kitagawa, S. Nanochannels of Two Distinct Cross-Sections in a Porous Al-Based Coordination Polymer. *J. Am. Chem. Soc.* 2008, 130, 13664–13672.
- (45) Liu, B.; Shioyama, H.; Akita, T.; Xu, Q. Metal-Organic Framework as a Template for Porous Carbon Synthesis. *J. Am. Chem. Soc.* 2008, 130, 5390–5391.
- (46) Zuo, T. T.; Wu, X. W.; Yang, C. P.; Yin, Y. X.; Ye, H.; Li, N. W.; Guo, Y. G. Graphitized Carbon Fibers as Multifunctional 3D Current Collectors for High Areal Capacity Li Anodes. *Adv. Mater.* 2017, 29, No. 1700389.
- (47) Yan, K.; Lu, Z.; Lee, H. W.; Xiong, F.; Hsu, P. C.; Li, Y.; Zhao, J.; Chu, S.; Cui, Y. Selective Deposition and Stable Encapsulation of Lithium Through Heterogeneous Seeded Growth. *Nat. Energy* 2016, 1, No. 16010.
- (48) Zheng, J.; Engelhard, M. H.; Mei, D.; Jiao, S.; Polzin, B. J.; Zhang, J. G.; Xu, W. Electrolyte Additive Enabled Fast Charging and Stable Cycling Lithium Metal Batteries. *Nat. Energy* 2017, 2, No. 17012.
- (49) Yang, C. P.; Yin, Y. X.; Zhang, S. F.; Li, N. W.; Guo, Y. G. Accommodating Lithium into 3D Current Collectors with a Submicron Skeleton Towards Long-Life Lithium Metal Anodes. *Nat. Commun.* 2015, 6, No. 8058.
- (50) Cheng, X. B.; Hou, T. Z.; Zhang, R.; Peng, H. J.; Zhao, C. Z.; Huang, J. Q.; Zhang, Q. Dendrite-Free Lithium Deposition Induced by Uniformly Distributed Lithium Ions for Efficient Lithium Metal Batteries. *Adv. Mater.* 2016, 28, 2888–2895.
- (51) Enslin, D.; Stjern Dahl, M.; Nyten, A.; Gustafsson, T.; Thomas, J. O. A Comparative XPS Surface Study of Li₂FeSiO₄/C Cycled with LiTFSI and LiPF₆-Based Electrolytes. *J. Mater. Chem.* 2009, 19, 82–88.
- (52) Sharova, V.; Moretti, A.; Diemant, T.; Varzia, A.; Behma, R. J.; Passerini, S. Comparative Study of Imide-Based Li Salts as Electrolyte Additives for Li-Ion Batteries. *J. Power Sources* 2018, 375, 43–52.
- (53) Aurbach, D.; Gamolsky, K.; Markovsky, B.; Gofer, Y.; Schmidt, M.; Heider, U. On the Use of Vinylene Carbonate (VC) as an Additive to Electrolyte Solutions for Li-Ion Batteries. *Electrochim. Acta* 2002, 47, 1423–1439.
- (54) Zheng, J. M.; Yan, P. F.; Mei, D. H.; Engelhard, M. H.; Cartmell, S. S.; Polzin, B. J.; Wang, C. M.; Zhang, J. G.; Xu, W. Highly Stable Operation of Lithium Metal Batteries Enabled by the Formation of a Transient High-Concentration Electrolyte Layer. *Adv. Energy Mater.* 2016, 6, No. 1502151.
- (55) Li, Q.; Zhu, S.; Lu, Y. 3D Porous Cu Current Collector/LiMetal Composite Anode for Stable Lithium-Metal Batteries. *Adv. Funct. Mater.* 2017, 27, No. 1606422.